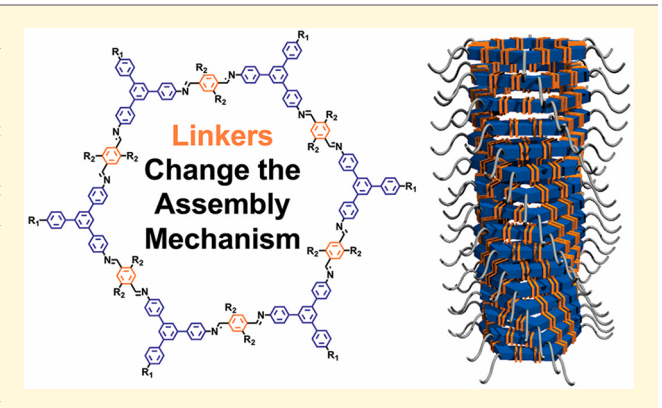


# Pathway Complexity in the Stacking of Imine-Linked Macrocycles Related to Two-Dimensional Covalent Organic Frameworks

Shiwei Wang,<sup>†,#</sup> Anton D. Chavez,<sup>†,§,#</sup> Simil Thomas,<sup>‡</sup> Hong Li,<sup>‡</sup> Nathan C. Flanders,<sup>†</sup> Chao Sun,<sup>†,§</sup> Michael J. Strauss,<sup>†</sup> Lin X. Chen,<sup>†,||</sup> Albert J. Markvoort,<sup>⊥</sup> Jean-Luc Bredas,<sup>‡</sup> and William R. Dichtel\*, 10

# Supporting Information

ABSTRACT: Interlayer interactions play an important role in the formation of two-dimensional covalent organic frameworks (2D COFs), yet the effects of monomer structure on COF formation, crystallinity, and susceptibility to exfoliation are not well understood. Here we probe these effects by studying the stacking behavior of imine-linked macrocycles that represent discrete models of 2D COFs. Specifically, macrocycles based on terephthaldehyde (PDA) or 2,5-dimethoxyterephthaldehyde (DMPDA) stack upon cooling molecularly dissolved solutions. Both macrocycles assemble cooperatively with similar  $\Delta H_e$  values of -97 kJ/mol and -101 kJ/mol, respectively, although the DMPDA macrocycle assembly process showed a more straightforward temperature dependence. Density functional theory calculations of the stacking of PDA macrocycles suggested



two stable configurations that were close in energy. Circular dichroism spectroscopy performed on macrocycles bearing chiral side chains revealed a helix reversion process for the PDA macrocycles that was not observed for the DMPDA macrocycles. Given the structural similarity of these monomers, these findings demonstrate that the stacking processes associated with nanotubes derived from these macrocycles, as well as for the corresponding COFs, are complex and susceptible to kinetic traps, casting doubt on the relevance of thermodynamic arguments for improving materials quality. Rather, a deeper understanding of the mechanism of supramolecular polymerization and its interplay with polymerization and error correction during COF synthesis is needed for improved control of the crystallinity and morphology of these emerging materials.

## ■ INTRODUCTION

Two-dimensional covalent organic frameworks (2D COFs) are crystalline polymers with periodic bonding in two orthogonal directions that are typically isolated as microcrystalline powders with layered structures. 1-4 Because of their designed topology and permanent porosity, these materials are of interest for applications such as gas storage, 5,6 optoelectronics,<sup>7,8</sup> electrical energy storage devices,<sup>9–12</sup> catalysis,<sup>13–15</sup> and filtration membranes.<sup>16–18</sup> Although 2D COF formation is not yet fully understood, interlayer interactions almost certainly play an important role, and strengthening them has been invoked in the design of structures with improved materials quality and stability. 19,20 However, the strength of these interlayer interactions is difficult to measure experimentally, and both electron-rich and electron-poor

aromatic aldehydes have produced highly crystalline iminelinked structures. Although differences in the crystallinity of different 2D COF structures have been rationalized by the more crystalline material having stronger interlayer interactions, 13 follow-up reports have demonstrated equal or better crystallinity of structures lacking these design criteria through modification of the polymerization conditions 19,23 or superior catalysis.<sup>24</sup> These observations suggest that 2D COF formation

Special Issue: Jean-Luc Bredas Festschrift

Received: August 1, 2019 Revised: August 8, 2019 Published: August 9, 2019



Department of Chemistry, Northwestern University, 2145 Sheridan Road, Evanston, Illinois 60208, United States

<sup>\*</sup>School of Chemistry and Biochemistry, Center for Organic Photonics and Electronics (COPE), Georgia Institute of Technology, Atlanta, Georgia 30332-0400, United States

<sup>§</sup>Department of Chemistry and Chemical Biology, Baker Laboratory, Cornell University, Ithaca, New York 14853, United States Chemical Sciences and Engineering Division, Argonne National Laboratory, Argonne, Illinois 60439, United States

<sup>&</sup>lt;sup>1</sup>Institute for Complex Molecular Systems and Computational Biology Group, Eindhoven University of Technology, P.O. Box 513, 5600 MB Eindhoven, The Netherlands

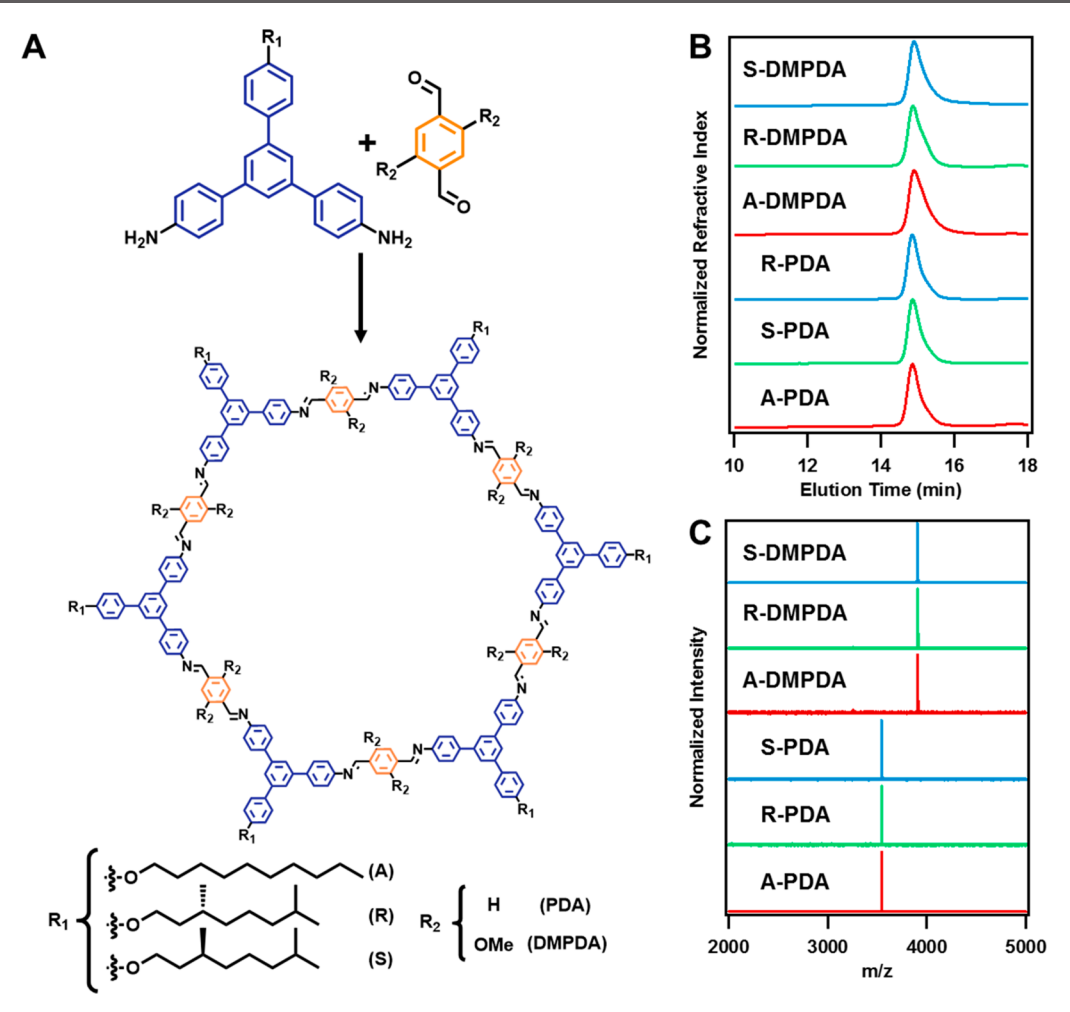


Figure 1. (A) Synthesis of achiral and chiral imine-linked macrocycles from the condensation of truncated TAPB analogues with either PDA or DMPDA. (B) Gel permeation chromatography traces of each macrocycle in THF. (C) MALDI-MS of each isolated macrocycle.

involves kinetic traps that complicate design conclusions based on stacking energies or other thermodynamic arguments. <sup>25–27</sup>

The study of COF formation is complicated by the insolubility of COFs upon polymerization, with studies of their formation as stable colloids a recent and notable exception.<sup>27-29</sup> Soluble or dispersible model systems of COFs are therefore of interest to better understand COF growth processes. We previously reported boronate esterlinked and imine-linked macrocycles whose dynamic bond formation and assembly are analogous to those of the corresponding 2D COFs. 25,26 For example, boronate esterlinked macrocycles showed hallmarks of nucleation-elongation processes also found in 2D COFs comprised of similar monomers. 19,25 Likewise, imine-linked macrocycles form via an initial linear polymerization, followed by the formation of layered aggregates that mimic how imine-linked 2D COFs crystallize under similar conditions. 26,27 Given the importance of stacking to drive macrocycle formation during their synthesis, we hypothesized that studying macrocycle assembly in the absence of transimination catalysts would provide insight into the relative strengths of COF interlayer interactions and the ways in which layered structures form in systems of higher dimensionality.

Here we report the synthesis and self-assembly of two types of imine-linked macrocycles containing either terephthaldehyde (PDA) or dimethoxyterephthaldehyde (DMPDA) condensed with truncated analogues of 1,3,5-tris(4aminophenyl)benzene (TAPB, Figure 1). These macrocycles serve as direct analogues of TAPB-PDA-COF, which has been the subject of mechanistic studies, 23,24,27,29,30 and the TAPB-DMPDA-COF reported by Jiang and co-workers. 13 Highly crystalline samples of the TAPB-DMPDA-COF were first obtained under polymerization conditions that provide only weakly crystalline and low surface area samples of TAPB-PDA-COF, and it was initially proposed that the electron-donating methoxy groups of DMPDA induce stronger interlayer interactions and enhanced crystallinity. However, highly crystalline samples of TAPB-PDA-COF were later obtained by other means, 19,29 including the use of Lewis acid catalysts 24 and transimination reactions.<sup>23</sup> With questions about the role of stacking in the two COFs unresolved, we studied the selfassembly of macrocycles by UV-vis spectroscopy, as well as circular dichroism (CD) spectroscopy of macrocycles bearing chiral side chains. Upon cooling, both macrocycles cooperatively stack from a molecularly dissolved state. van't Hoff analysis reveals similar  $\Delta H_e$  and  $\Delta S_e$  values for the achiral macrocycles, showing that the incorporation of dimethoxy groups does not significantly stabilize macrocycle stacking. However, the PDA and DMPDA assemblies form through different kinetic pathways, as evident from a difference in their assembly as a function of cooling rate in achiral derivatives and a helix reversion process observed for chiral PDA macrocycles

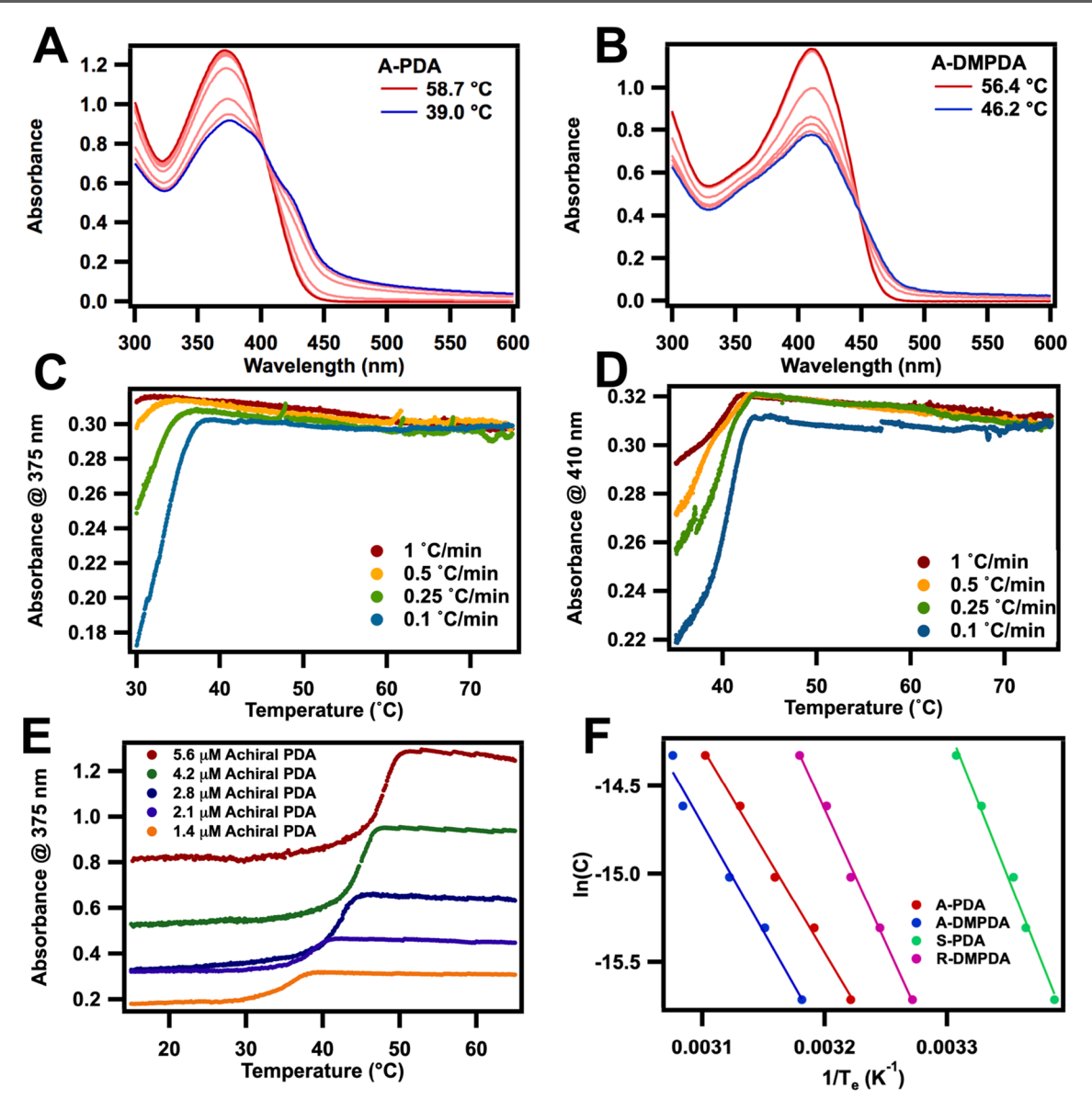


Figure 2. UV—vis spectra of (A) A-PDA and (B) A-DMPDA (5.6  $\mu$ M in 1:1 (v/v) DCE:toluene) cooled at 0.1 °C/min from 75 °C. Light red traces are seven evenly divided steps between the high (dark red) and low (blue) temperatures. (C) Absorbance intensity of the red-shifted shoulder (monitored at 375 nm) of solutions of A-PDA (1.4  $\mu$ M in 1:1 (v/v) DCE:toluene) cooled at various rates. (D) Absorbance intensity of the red-shifted shoulder (monitored at 410 nm) of A-DMPDA solutions (1.4  $\mu$ M in 1:1 (v/v) DCE:toluene) cooled at various rates. (E) Absorbance intensity of the red-shifted shoulder (monitored at 375 nm) of solutions of A-PDA (various concentrations in 1:1 (v/v) DCE:toluene) cooled at 0.1 °C/min. (F) van't Hoff plot for A-PDA, A-DMPDA, S-PDA, and R-DMPDA macrocycles. Concentrations are in molar fractions.

that is not observed for chiral DMPDA macrocycles. These studies reveal distinct and complex assembly mechanisms, even for these structurally similar macrocycles. A deeper understanding of the mechanisms of noncovalent assembly will greatly benefit our ability to control and manipulate polymerization processes in two or three dimensions, as well as the one-dimensional assembly of large macrocycles into nanotubes.<sup>31</sup>

#### **■** EXPERIMENTAL SECTION

**Synthesis.** Macrocycles were synthesized from diamine and dialdehyde monomers (Figure 1) in 1,4-dioxane (30 mM of both components) in a 4 mL closed vial under catalysis of  $CF_3CO_2H$  (10 equiv for R/S-PDA, 0.5 equiv for all others). The solutions were left to sit for 1–6 days before being neutralized with  $Et_3N$  (50 equiv for R/S-PDA, 10 equiv for all others). The precipitate was then resuspended, rinsed, and centrifuged with  $Et_2O$  (15 mL  $\times$  3),

EtOAc (15 mL  $\times$  1), hexane (15 mL  $\times$  1), and anhydrous acetone (15 mL  $\times$  1). The orange solid was dried under high vacuum at room temperature. Acyclic polymer poly-A-PDA was synthesized in ethyl acetate (60 mM of both components) with CF<sub>3</sub>CO<sub>2</sub>H (0.2 equiv). The reaction was terminated after 3 min by the addition of Et<sub>3</sub>N (1.2 equiv). The yellow solid was then washed with the same procedure and dried under vacuum at room temperature. Material quality was confirmed with gel permeation chromatography (GPC), matrix assisted laser desorption ionization time-of-flight mass spectrometry (MALDI-TOF), and nuclear magnetic resonance (NMR) spectroscopy.

**Solution Preparation.** Macrocycles were suspended under sonication and stocked in anhydrous toluene (0.4 mg/mL, JC Meyer System). The solution was then mixed with an equal volume of 1,2-dichloroethane (dried with molecular sieves) and diluted to desired concentration.

UV-Vis and van't Hoff Analysis. Macrocycle solution was added to a 1 cm cuvette and monitored under UV-vis during cooling

at 0.1 °C/min. The solution was constantly stirred at around 60 rpm. Elongation temperature ( $T_{\rm e}$ ) was determined by performing a nonlinear least-squares analysis using the method developed by Markvoort et al.<sup>35</sup> and ten Eikelder et al.<sup>36</sup> Accurate  $T_{\rm e}$  values were obtained by applying a weight of 10 at  $T_{\rm e}$  ( $\Delta T=1$ ). Linear regression of van't Hoff analysis was conducted with Igor Pro 6.37.

**Theoretical Computations.** The calculations were performed with the tuned long-range corrected  $\omega$ B97X-D functional and the 6-31G(d,p) basis set, using the Gaussian 09 Revision D.01 suite of programs.

**Circular Dichroism (CD) Analysis.** Macrocycle solutions were heated at 75 °C for 15 min and cooled at room temperature ambiently before measurement at 20 °C in a 1 cm path-length cuvette. Measurements are taken with standard sensitivity, D.I.T. at 1 s, bandwidth at 1 nm, data pitch at 1 nm, from 600 to 300 nm, and without accumulations.

#### ■ RESULTS AND DISCUSSION

PDA and DMPDA-containing macrocycles were obtained by condensing the corresponding dialdehyde with a truncated analogue of typical COF monomer, 1,3,5-tris(4-aminophenyl)-benzene, here capped with either achiral (A) decyloxy or chiral (R or S) 3,7-dimethylalkoxy groups (Figure 1A). These macrocycles are formed in high yields and selectivities for the hexagonal macrocycle, as shown by single distributions of monodisperse peaks eluting at ~15 min by GPC (Figure 1B) and the corresponding MALDI-MS [M + H] $^+$  adducts of the two types of macrocycles at 3543 and 3905 m/z for the PDA and DMPDA-containing macrocycles, respectively (Figure 1C). The macrocycles were also characterized by NMR spectroscopy (see Supporting Information), which was consistent with their 6-fold symmetric structures.

The PDA and DMPDA macrocycles assemble from the molecularly dissolved state into layered structures when anhydrous toluene:1,2-dichloroethane solutions (v/v = 1:1, 1.4–5.6  $\mu$ M) are cooled from 75 °C to room temperature. Both PDA and DMPDA macrocycles are monomeric at temperatures above 50 °C, with absorbance maxima at  $\lambda_{\text{max}}$  = 375 and 410 nm, respectively (Figure 2A,B). Upon cooling, the spectra of both types of macrocycles exhibit decreased absorbance intensity at  $\lambda_{max}$  and the appearance of a redshifted shoulder with a corresponding isosbestic point at 403 nm for A-PDA and 448 nm for A-DMPDA. Dynamic light scattering confirms that these spectral changes are associated with macrocycle aggregation (Figures S1-S3). Drop-cast films of macrocycle solutions at room temperature revealed fibrous structures, as observed by atomic force microscopy (AFM), further confirming that the macrocycles aggregate under these conditions (Figures S4 and S5). Furthermore, a linear iminelinked polymer independently prepared from the achiral TAPB analogue and PDA did not show the same spectral changes upon cooling, indicating that differences in the UV-vis spectra are due to supramolecular interactions between macrocycles rather than acyclic imine-linked structures (Figure S6). These combined observations suggest that both types of macrocycles stack cofacially into extended structures as their solutions are cooled.

To obtain a first understanding of the stacking of unfunctionalized macrocycles, we optimized the stacking geometry of a dimer of TAPB-PDA. The calculations were performed at the density functional theory (DFT) level using the tuned long-range-corrected  $\omega$ B97X-D functional, which includes dispersion interactions, and the 6-31G(d,p) basis set (see Supporting Information). Note that, since we are

interested in the backbone—backbone interactions and given the size of the dimer, the alkyl chains ( $R_1$  in Figure 1) were replaced as hydrogens in the calculations. We considered four starting geometries by placing the two macrocycles exactly on top of one another (1), which corresponds to an eclipsed configuration, as well as on top of one another with the upper macrocycle rotated by  $10^{\circ}(2)$ ,  $20^{\circ}$  (3), or  $30^{\circ}$  (4) with respect to the bottom macrocycle. Given the approximate 6-fold symmetry of each macrocycle, these initial geometries provide for a comprehensive set of starting conditions. After full optimization, the starting configuration (1) leads to the largest dimer binding energy, on the order of 516.7 kJ/mol. To reduce the repulsion effects that are associated with a perfectly eclipsed situation, the upper ring displaces slightly over the course of the optimization, by some 0.4 Å (Figure 3A); the

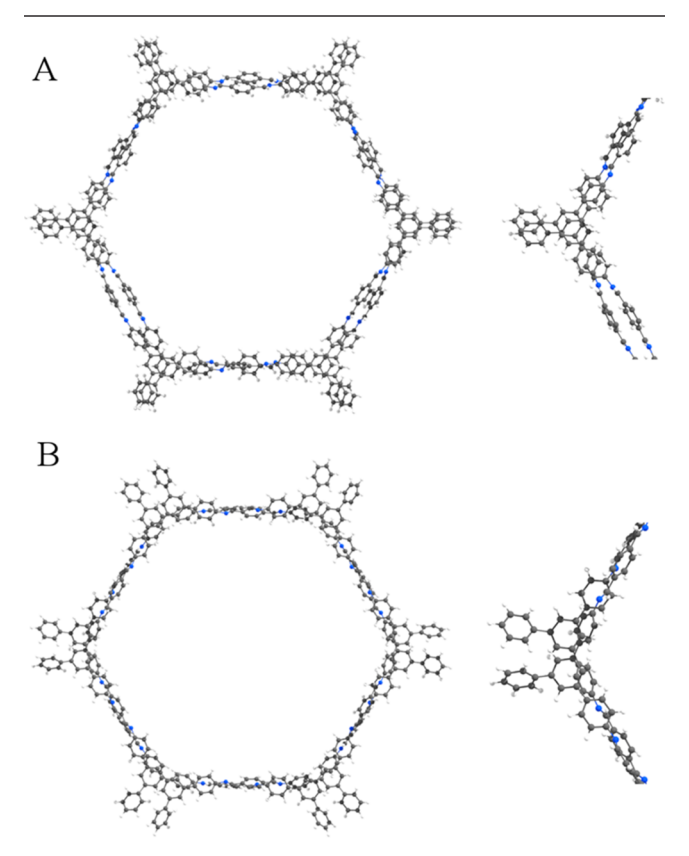


Figure 3. Geometry of the TAPB-PDA macrocycle dimer optimized at the  $\omega$ B97X-D level: (A) displaced-eclipsed configuration and (B) rotated configuration (color coding is gray for carbon, white for hydrogen, and blue for nitrogen).

average distance between lower and upper phenylene rings is ca. 3.98 Å. However, the other three starting configurations converge into the same dimer geometry, corresponding to a rotation of the upper macrocycle by 9° (Figure 3B). Here, the binding energy is only slightly smaller than in optimized configuration (1), 502.1 kJ/mol. Thus, the two optimized geometries are thermodynamically very similar in energy, which suggests that the identity and nature of interactions among solubilizing groups could stabilize one with respect to the other. It is also possible that these configurations are similar enough in energy that kinetic effects could influence which form is obtained under various assembly conditions. These dimer binding energies roughly translate into interaction energies between two stacked phenylene rings of some 14 kJ/

mol, which is consistent with the binding energies found in benzene dimers.<sup>34</sup> It must be borne in mind that the binding energies calculated here are specific to isolated dimers. When addressing stacking energies in solution (see below), the values are expected to be significantly smaller since the formation of a macrocycle dimer in solution implies a loss of macrocycle—solvent interactions.

To further investigate the mechanism of macrocycle aggregate formation, we evaluated the macrocycle assembly as a function of cooling rate and concentration. The change in absorbance at each macrocycle's  $\lambda_{max}$  (375 nm for PDA and 410 nm for DMPDA) was plotted as a function of temperature at various cooling rates (Figure 2C,D). At the slowest cooling rate (0.1 °C/min), a sudden change in absorbance at a specific temperature (Te, elongation temperature) indicates that both PDA and DMPDA macrocycles assemble cooperatively. Prior to assembly, there is a small increase in absorbance, which we attribute to an increase in the average conjugation as the temperature decreases from 75 °C to  $T_e$ . This phenomenon is also consistent with fluorescence spectroscopy, which shows a red shift in emission as the macrocycles are cooled from 75 to 48 °C (Figure S7). The rate of cooling has a significant effect on the overall shape of the cooling curve. For PDA macrocycles, slower cooling rates give rise to higher Te and greater absorbance changes (Figure 2C). The A-PDA solutions cooled at 1  $^{\circ}$ C/min exhibited a  $T_e$  of 28.8  $^{\circ}$ C and  $T_e$  of 36.5 °C when cooled at 0.1 °C/min. This cooling rate dependence suggests the formation of kinetically trapped assemblies. In contrast, A-DMPDA macrocycles have similar  $T_e$  values at each cooling rate, ranging from 41.9 °C at 1 °C/min to 42.9 °C at 0.1 °C/min (Figure 2D). We hypothesized that this discrepancy is due to PDA's more complex kinetic behavior, which is consistent with the circular dichroism studies of chiral macrocycles described below. However, even though A-DMPDA macrocycles have similar  $T_e$  at each cooling rate, we were unable to reach the thermodynamic state of macrocycle assembly for either macrocycle, at which the same T<sub>e</sub> value and absorbance change would be observed for different cooling rates. Because the self-assembly of macrocycles is pathway-dependent, all cooling curves for thermodynamic analysis were generated at the slowest cooling rate of 0.1 °C/min.

A van't Hoff analysis of cooling curves collected at different macrocycle concentrations was performed to determine thermodynamic assembly parameters. A-PDA and A-DMPDA were heated to 75 °C and then cooled to 10 °C at 0.1 °C/min, and these experiments were performed at five macrocycle concentrations (Figures 2E and S8). Due to the observed redshift, fitting the cooling curves to the nucleationelongation model developed by Markvoort et al.35 and ten Eikelder et al.<sup>36</sup> resulted in significant deviation at low temperatures (Figure S9). 37,38 However, these deviations do not perturb the determination of the  $T_e$  values, which are used in the van't Hoff analysis<sup>39</sup> for A-PDA, A-DMPDA, S-PDA, and R-DMPDA. We obtained  $\Delta H_e$  values of  $-97 \pm 4$  kJ/mol and  $-101 \pm 7$  kJ/mol, for A-PDA and A-DMPDA, respectively (Figure 2F, Table 1). The similarity of these values indicates that there is little to no enthalpic gain in macrocycle aggregation for DMPDA compared to PDA. Although this observation is in contrast with previously reported theoretical values for the corresponding COFs calculated at the DFT-B level, 13 it is consistent with the description coming from stateof-the-art quantum chemistry calculations by Sherrill, 40 which

Table 1. Thermodynamic Parameters of Macrocycle Assembly

	achiral PDA	achiral DMPDA	chiral PDA	chiral DMPDA
$\frac{\Delta H_{ m e}}{({ m kJ/mol})}$	$-97 \pm 4$	$-101 \pm 7$	$-145 \pm 8$	$-127 \pm 5$
$\frac{\Delta S_{\rm e}}{({ m J/mol\cdot K})}$	$-181 \pm 11$	$-192 \pm 23$	$-360 \pm 26$	$-282 \pm 17$
$R^2$	0.996	0.984	0.991	0.995

point to the subtle balance between dispersion and electrostatic effects when considering the impact of electron-accepting or electron-donating substituents on stacking enthalpies. Chiral alkyl side chains significantly increased the elongation entropies and enthalpies for both PDA and DMPDA, potentially by inducing more ordered assemblies with increased interactions among the chiral alkyl side chains.

When functionalized with enantiopure chiral alkoxy groups, PDA and DMPDA macrocycles assemble into helical structures that show distinct kinetic behavior. Four macrocycles were investigated, each with 3,7-dimethyloctyloxy side chains of either (R) or (S) configuration, including both PDA and DMPDA structures. Solutions of each macrocycle (2.8 μM, 1:1 DCE:toluene) showed silent circular dichroism (CD) spectra at 75 °C (Figure S10), but strong CD signals emerged and stabilized upon cooling and standing at room temperature for 3 hours. S-PDA and R-PDA exhibit mirror-image CD spectra, whereas achiral A-PDA remains CD silent, and the same phenomena are observed for DMPDA macrocycles (Figure 4A,B). S-PDA exhibits a positive Cotton effect at 300 to 430 nm and a negative Cotton effect from 430 to 600 nm (Figure 4A), while S-DMPDA exhibits a negative Cotton effect from 300 to 463 nm and a positive Cotton effect at 463 to 600 nm (Figure 4B), suggesting PDA and DMPDA ultimately form assemblies of opposite helicity under the influence of the same chiral alkyl side chains. To further explore why the DMPDA and PDA macrocycles form assemblies of opposite helicity, CD spectra of S-PDA and S-DMPDA were obtained as a function of time, beginning immediately after the solutions were cooled to 20 °C (Figures 4C,D and S11). The spectral evolution of the S-DMPDA solution was straightforward, with the spectra intensifying but always maintaining the positive feature centered at 478 nm and negative feature centered at 420 nm, corresponding to the formation of the structures observed after longer times (Figure 4D). In contrast, spectra of the S-PDA macrocycle initially showed similar behavior to those of the S-DMPDA. However, the intensity of these peaks reached a maximum at 35 min, after which they transformed into the spectrum of opposite helicity obtained at extended times (Figure 4C). This behavior corresponds to the rapid formation of one helical superstructure, which undergoes reversion to a more stable helical assembly (Figure 4E). Helix reversions have been observed as kinetic products during the formation of other chiral supramolecular assemblies. 32,38,41-43 In these macrocycles, we hypothesize that both PDA and DMPDA form the same initial kinetic product but that only the PDA macrocycles undergo the helix reversion. This difference may arise from the steric effects of the dimethoxy groups, which could limit the rotations of layered macrocycles. These differences in the chiral systems may also explain the differences observed in the elongation temperatures in the achiral macrocycles.

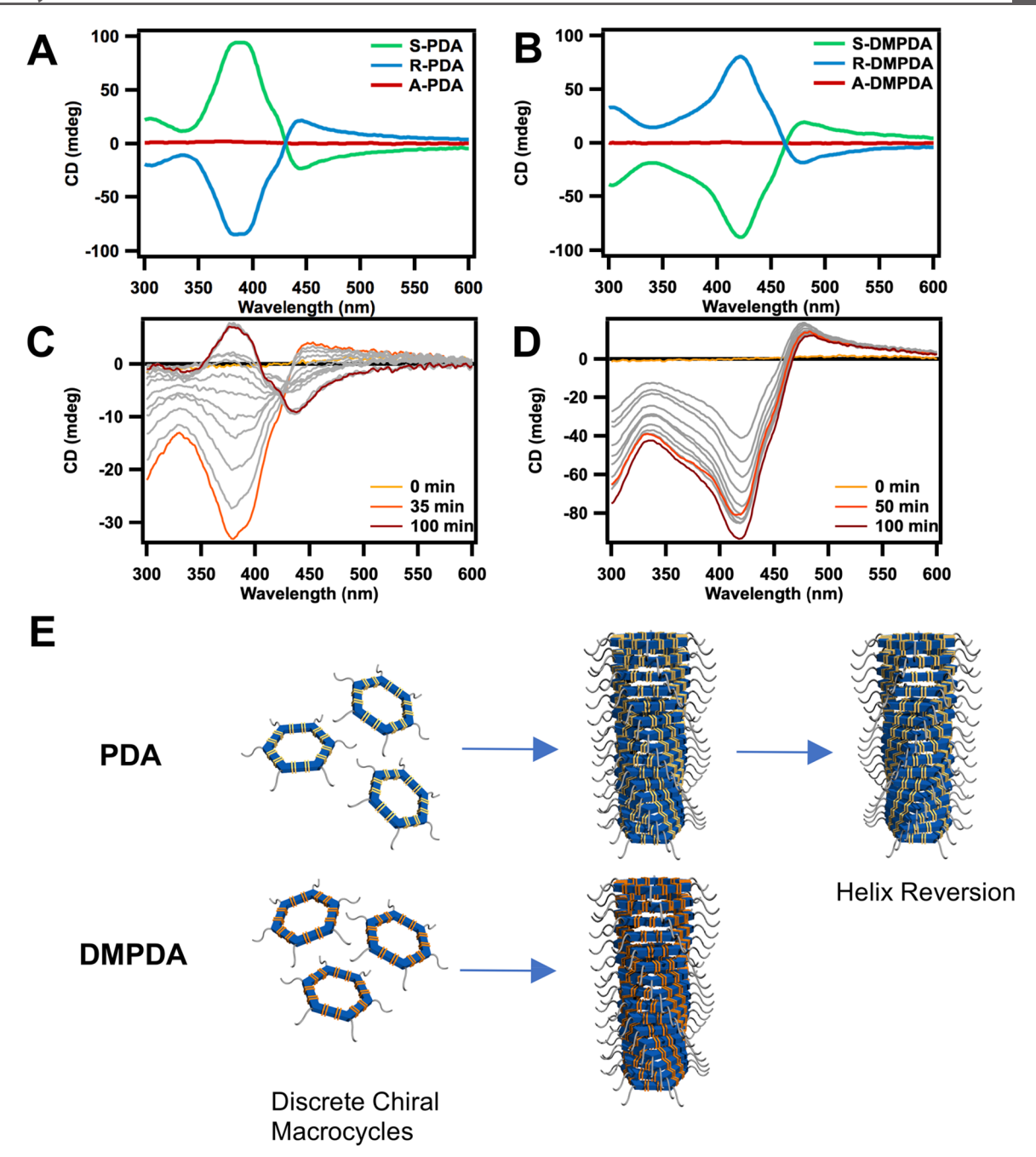


Figure 4. (A, B) CD spectra of PDA and DMPDA macrocycle solutions (2.8  $\mu$ M in 1:1 DCE:toluene) after cooling to 20 °C and standing for 3 h. (C) CD spectra of S-PDA (2.8  $\mu$ M in 1:1 DCE:toluene) at 0, 35, and 100 min after cooling at 20 °C. Gray traces show the evolution of the spectra at 5 min increments between 35 and 100 min. (D) CD spectra of S-DMPDA (2.8  $\mu$ M in 1:1 DCE:toluene) at 0, 50, and 100 min after cooling at 20 °C. Gray traces show the evolution of the spectra at 5 min increments between 0 and 50 min. (E) Scheme of chiral self-assembly of PDA and DMPDA.

# CONCLUSIONS

We have studied the assembly of imine-linked hexagonal macrocycles, in part to gain insight into the stacking of closely related 2D COFs. Upon identifying appropriate conditions for the assembly of PDA and DMPDA macrocycles, it was found that both were molecularly dissolved at 75 °C and stack cooperatively upon cooling. DFT calculations identified two energy minima conformations of PDA macrocycles without significant energy differences, suggesting that they might be susceptible to kinetic effects. The stacking of A-PDA is highly dependent on the cooling rate, as evidenced by shifts in the

observed elongation temperature. In contrast, the elongation temperature of the A-DMPDA macrocycle assembly is much less dependent on the cooling rate. When cooled at 0.1 °C/min, the elongation enthalpy and entropy of A-PDA and A-DMPDA were determined using a van't Hoff analysis based on changes in elongation temperature as a function of macrocycle concentration. Similar values of enthalpy and entropy were acquired for both macrocycles, suggesting that the methoxy groups do not stabilize stacking thermodynamically. PDA and DMPDA macrocycles bearing chiral side chains exhibit distinct assembly behavior, with PDA undergoing a helix reversion that is not observed for DMPDA. We hypothesize that the methoxy

groups interdigitate during stacking, which prevents the stacked DMPDA macrocycles from undergoing helix reversion to the thermodynamic assembly. The PDA macrocycle's more complex kinetic processes may also explain the dependence on cooling rate observed in achiral PDA macrocycle elongation.

These experiments demonstrate that the introduction of methoxy groups hardly changes the thermodynamic properties of interlayer interactions among macrocycles but does alter the kinetic process of self-assembly. Although previous COF studies have used calculated stacking energy to justify the formation of highly crystalline products, our findings suggest that kinetic processes associated with the formation of lavered structures may more strongly affect materials quality. These model systems deepen our understanding of interlayer interactions crucial to the formation of nanotubes and COFs. The studies also contribute to the critical mechanistic understanding of noncovalent synthesis, including aspects of monomer functionalization and programmed supramolecular control (such as temperature, concentration, reaction time, and monomer addition rate), to achieve ordered, dynamic, and, ultimately, functional molecular assemblies.

## ASSOCIATED CONTENT

# Supporting Information

The Supporting Information is available free of charge on the ACS Publications website at DOI: 10.1021/acs.chemmater.9b03088.

Materials and instrumentation parameters, computational methodology, synthetic procedure of macrocycles and monomers, DLS correlograms of macrocycle solutions at different temperatures, AFM image of drop-casted samples, UV—vis traces of poly-A-PDA as well as macrocycle solutions during cooling, fluorescent spectra of A-PDA solution during cooling, circular dichroism spectra of macrocycle solutions at 75 °C and 5 min after cooling, and NMR spectra of monomers and macrocycles (PDF)

## AUTHOR INFORMATION

## **Corresponding Author**

\*(W.R.D.) E-mail: wdichtel@northwestern.edu.

ORCID ®

Shiwei Wang: 0000-0002-6097-3424 Hong Li: 0000-0002-4513-3056 Chao Sun: 0000-0002-0542-5935

Michael J. Strauss: 0000-0003-0808-2568 Albert J. Markvoort: 0000-0001-6025-9557 Jean-Luc Bredas: 0000-0001-7278-4471 William R. Dichtel: 0000-0002-3635-6119

## **Author Contributions**

\*(S.W. and A.D.C.) These authors contributed equally.

## Notes

The authors declare no competing financial interest.

# ACKNOWLEDGMENTS

This work was funded by the Army Research Office through the Multidisciplinary University Research Initiative (MURI, W911NF-15-1-0447, to W.R.D. and J.-L.B.). A.D.C. was supported through a National Defense Science and Engineering Graduate Fellowship (NDSEG). S.W. was supported partially by the Northwestern University Summer Under-

graduate Research Grant and Weinberg College Summer Undergraduate Research Grant. C.S. was partially supported by the Cornell Center for Materials Research with funding from the NSF MRSEC program (DMR-1719875). This work made use of the Integrated Molecular Structure Education and Research Center (IMSERC) at Northwestern University, which has received support from the National Science Foundation (NSF; (CHE 1048773), the Soft and Hybrid Nanotechnology Experimental (SHyNE) Resource (NSF NNCI 1542205), the State of Illinois, and the International Institute for Nanotechnology (IIN)). This work was supported in part by a grant of computer time from the DOD High Performance Computing Modernization Program.

## REFERENCES

- (1) DeBlase, C. R.; Dichtel, W. R. Moving Beyond Boron: The Emergence of New Linkage Chemistries in Covalent Organic Frameworks. *Macromolecules* **2016**, 49 (15), 5297–5305.
- (2) Bisbey, R. P.; Dichtel, W. R. Covalent Organic Frameworks as a Platform for Multidimensional Polymerization. *ACS Cent. Sci.* **2017**, *3* (6), 533–543.
- (3) Jin, Y.; Hu, Y.; Zhang, W. Tessellated Multiporous Two-Dimensional Covalent Organic Frameworks. *Nat. Rev. Chem.* **2017**, *1* (7), 0056.
- (4) Huang, N.; Wang, P.; Jiang, D. Covalent Organic Frameworks: A Materials Platform for Structural and Functional Designs. *Nat. Rev. Mater.* **2016**, *1* (10), 16068.
- (5) Zeng, Y.; Zou, R.; Zhao, Y. Covalent Organic Frameworks for CO<sub>2</sub> Capture. *Adv. Mater.* **2016**, 28 (15), 2855–2873.
- (6) Huang, N.; Chen, X.; Krishna, R.; Jiang, D. Two-Dimensional Covalent Organic Frameworks for Carbon Dioxide Capture through Channel-Wall Functionalization. *Angew. Chem., Int. Ed.* **2015**, 54 (10), 2986–2990.
- (7) Chen, L.; Furukawa, K.; Gao, J.; Nagai, A.; Nakamura, T.; Dong, Y.; Jiang, D. Photoelectric Covalent Organic Frameworks: Converting Open Lattices into Ordered Donor-Acceptor Heterojunctions. *J. Am. Chem. Soc.* **2014**, *136* (28), 9806–9809.
- (8) Guo, J.; Xu, Y.; Jin, S.; Chen, L.; Kaji, T.; Honsho, Y.; Addicoat, M. A.; Kim, J.; Saeki, A.; Ihee, H. Conjugated Organic Framework with Three-Dimensionally Ordered Stable Structure and Delocalized  $\pi$  Clouds. *Nat. Commun.* **2013**, *4*, 2736.
- (9) DeBlase, C. R.; Silberstein, K. E.; Truong, T.-T.; Abruña, H. D.; Dichtel, W. R.  $\beta$ -Ketoenamine-Linked Covalent Organic Frameworks Capable of Pseudocapacitive Energy Storage. *J. Am. Chem. Soc.* **2013**, 135 (45), 16821–16824.
- (10) DeBlase, C. R.; Hernández-Burgos, K.; Silberstein, K. E.; Rodríguez-Calero, G. G.; Bisbey, R. P.; Abruña, H. D.; Dichtel, W. R. Rapid and Efficient Redox Processes within 2D Covalent Organic Framework Thin Films. *ACS Nano* **2015**, *9* (3), 3178–3183.
- (11) Mulzer, C. R.; Shen, L.; Bisbey, R. P.; McKone, J. R.; Zhang, N.; Abruña, H. D.; Dichtel, W. R. Superior Charge Storage and Power Density of a Conducting Polymer-Modified Covalent Organic Framework. ACS Cent. Sci. 2016, 2 (9), 667–673.
- (12) Halder, A.; Ghosh, M.; Khayum M, A.; Bera, S.; Addicoat, M.; Sasmal, H. S.; Karak, S.; Kurungot, S.; Banerjee, R. Interlayer Hydrogen-Bonded Covalent Organic Frameworks as High-Performance Supercapacitors. *J. Am. Chem. Soc.* **2018**, *140* (35), 10941–10945.
- (13) Xu, H.; Gao, J.; Jiang, D. Stable, Crystalline, Porous, Covalent Organic Frameworks as a Platform for Chiral Organocatalysts. *Nat. Chem.* **2015**, 7 (11), 905–912.
- (14) Han, X.; Xia, Q.; Huang, J.; Liu, Y.; Tan, C.; Cui, Y. Chiral Covalent Organic Frameworks with High Chemical Stability for Heterogeneous Asymmetric Catalysis. *J. Am. Chem. Soc.* **2017**, *139* (25), 8693–8697.
- (15) Lin, S.; Diercks, C. S.; Zhang, Y.-B.; Kornienko, N.; Nichols, E. M.; Zhao, Y.; Paris, A. R.; Kim, D.; Yang, P.; Yaghi, O. M.; et al.

Covalent Organic Frameworks Comprising Cobalt Porphyrins for Catalytic CO2 Reduction in Water. *Science* **2015**, 349 (6253), 1208–1213

- (16) Matsumoto, M.; Valentino, L.; Stiehl, G. M.; Balch, H. B.; Corcos, A. R.; Wang, F.; Ralph, D. C.; Mariñas, B. J.; Dichtel, W. R. Lewis-Acid-Catalyzed Interfacial Polymerization of Covalent Organic Framework Films. *Chem* **2018**, *4* (2), 308–317.
- (17) Valentino, L.; Matsumoto, M.; Dichtel, W. R.; Mariñas, B. J. Development and Performance Characterization of a Polyimine Covalent Organic Framework Thin-Film Composite Nanofiltration Membrane. *Environ. Sci. Technol.* **2017**, *51* (24), 14352–14359.
- (18) Yuan, S.; Li, X.; Zhu, J.; Zhang, G.; Van Puyvelde, P.; Van der Bruggen, B. Covalent Organic Frameworks for Membrane Separation. *Chem. Soc. Rev.* **2019**, 48 (10), 2665–2681.
- (19) Smith, B. J.; Hwang, N.; Chavez, A. D.; Novotney, J. L.; Dichtel, W. R. Growth Rates and Water Stability of 2D Boronate Ester Covalent Organic Frameworks. *Chem. Commun.* **2015**, *51* (35), 7532–7535.
- (20) Thompson, C. M.; Occhialini, G.; McCandless, G. T.; Alahakoon, S. B.; Cameron, V.; Nielsen, S. O.; Smaldone, R. A. Computational and Experimental Studies on the Effects of Monomer Planarity on Covalent Organic Framework Formation. *J. Am. Chem. Soc.* **2017**, *139* (30), 10506–10513.
- (21) Alahakoon, S. B.; McCandless, G. T.; Karunathilake, A. A. K.; Thompson, C. M.; Smaldone, R. A. Enhanced Structural Organization in Covalent Organic Frameworks Through Fluorination. *Chem. Eur. J.* 2017, 23 (18), 4255–4259.
- (22) Alahakoon, S. B.; Occhialini, G.; McCandless, G. T.; Karunathilake, A. A. K.; Nielsen, S. O.; Smaldone, R. A. Experimental and Theoretical Insight into the Effect of Fluorine Substituents on the Properties of Azine Linked Covalent Organic Frameworks. CrystEngComm 2017, 19 (33), 4882–4885.
- (23) Vitaku, E.; Dichtel, W. R. Synthesis of 2D Imine-Linked Covalent Organic Frameworks through Formal Transimination Reactions. *J. Am. Chem. Soc.* **2017**, *139* (37), 12911–12914.
- (24) Matsumoto, M.; Dasari, R. R.; Ji, W.; Feriante, C. H.; Parker, T. C.; Marder, S. R.; Dichtel, W. R. Rapid, Low Temperature Formation of Imine-Linked Covalent Organic Frameworks Catalyzed by Metal Triflates. J. Am. Chem. Soc. 2017, 139 (14), 4999–5002.
- (25) Chavez, A. D.; Smith, B. J.; Smith, M. K.; Beaucage, P. A.; Northrop, B. H.; Dichtel, W. R. Discrete, Hexagonal Boronate Ester-Linked Macrocycles Related to Two-Dimensional Covalent Organic Frameworks. *Chem. Mater.* **2016**, *28* (14), 4884–4888.
- (26) Chavez, A. D.; Evans, A. M.; Flanders, N. C.; Bisbey, R. P.; Vitaku, E.; Chen, L. X.; Dichtel, W. R. Equilibration of Imine-Linked Polymers to Hexagonal Macrocycles Driven by Self-Assembly. *Chem. Eur. J.* 2018, 24 (16), 3989–3993.
- (27) Smith, B. J.; Parent, L. R.; Overholts, A. C.; Beaucage, P. A.; Bisbey, R. P.; Chavez, A. D.; Hwang, N.; Park, C.; Evans, A. M.; Gianneschi, N. C.; et al. Colloidal Covalent Organic Frameworks. *ACS Cent. Sci.* 2017, 3 (1), 58–65.
- (28) Evans, A. M.; Parent, L. R.; Flanders, N. C.; Bisbey, R. P.; Vitaku, E.; Kirschner, M. S.; Schaller, R. D.; Chen, L. X.; Gianneschi, N. C.; Dichtel, W. R. Seeded Growth of Single-Crystal Two-Dimensional Covalent Organic Frameworks. *Science* **2018**, *361* (6397), 52–57.
- (29) Li, R. L.; Flanders, N. C.; Evans, A. M.; Ji, W.; Castano, I.; Chen, L. X.; Gianneschi, N. C.; Dichtel, W. R. Controlled Growth of Imine-Linked Two-Dimensional Covalent Organic Framework Nanoparticles. *Chem. Sci.* **2019**, *10* (13), 3796–3801.
- (30) Yuan, Y.-C.; Sun, B.; Cao, A.-M.; Wang, D.; Wan, L.-J. Heterogeneous Nucleation and Growth of Highly Crystalline Imine-Linked Covalent Organic Frameworks. *Chem. Commun.* **2018**, *54* (47), 5976–5979.
- (31) Sun, C.; Shen, M.; Chavez, A. D.; Evans, A. M.; Liu, X.; Harutyunyan, B.; Flanders, N. C.; Hersam, M. C.; Bedzyk, M. J.; Olvera de la Cruz, M.; et al. High Aspect Ratio Nanotubes Assembled from Macrocyclic Iminium Salts. *Proc. Natl. Acad. Sci. U. S. A.* **2018**, *115* (36), 8883–8888.

- (32) Korevaar, P. A.; George, S. J.; Markvoort, A. J.; Smulders, M. M. J.; Hilbers, P. A. J.; Schenning, A. P. H. J.; De Greef, T. F. A.; Meijer, E. W. Pathway Complexity in Supramolecular Polymerization. *Nature* **2012**, *481* (7382), 492–496.
- (33) Korevaar, P. A.; de Greef, T. F. A.; Meijer, E. W. Pathway Complexity in  $\pi$ -Conjugated Materials. *Chem. Mater.* **2014**, 26 (1), 576–586.
- (34) Sinnokrot, M. O.; Valeev, E. F.; Sherrill, C. D. Estimates of the Ab Initio Limit for  $\Pi$ - $\pi$  Interactions: The Benzene Dimer. *J. Am. Chem. Soc.* **2002**, 124 (36), 10887–10893.
- (35) Markvoort, A. J.; ten Eikelder, H. M. M.; Hilbers, P. A. J.; de Greef, T. F. A.; Meijer, E. W. Theoretical Models of Nonlinear Effects in Two-Component Cooperative Supramolecular Copolymerizations. *Nat. Commun.* **2011**, *2*, 509.
- (36) ten Eikelder, H. M. M.; Markvoort, A. J.; de Greef, T. F. A.; Hilbers, P. A. J. An Equilibrium Model for Chiral Amplification in Supramolecular Polymers. *J. Phys. Chem. B* **2012**, *116* (17), 5291–5301.
- (37) Stals, P. J. M.; Korevaar, P. A.; Gillissen, M. A. J.; de Greef, T. F. A.; Fitié, C. F. C.; Sijbesma, R. P.; Palmans, A. R. A.; Meijer, E. W. Symmetry Breaking in the Self-Assembly of Partially Fluorinated Benzene-1,3,5-Tricarboxamides. *Angew. Chem., Int. Ed.* **2012**, *51* (45), 11297–11301.
- (38) Adelizzi, B.; Filot, I. A. W.; Palmans, A. R. A.; Meijer, E. W. Unravelling the Pathway Complexity in Conformationally Flexible *N* -Centered Triarylamine Trisamides. *Chem. Eur. J.* **2017**, 23 (25), 6103–6110.
- (39) Jonkheijm, P.; van der Schoot, P.; Schenning, A. P. H. J.; Meijer, E. W. Probing the Solvent-Assisted Nucleation Pathway in Chemical Self-Assembly. *Science* **2006**, *313* (5783), 80–83.
- (40) Sherrill, C. D. Energy Component Analysis of  $\pi$  Interactions. *Acc. Chem. Res.* **2013**, 46 (4), 1020–1028.
- (41) Ogi, S.; Fukui, T.; Jue, M. L.; Takeuchi, M.; Sugiyasu, K. Kinetic Control over Pathway Complexity in Supramolecular Polymerization through Modulating the Energy Landscape by Rational Molecular Design. *Angew. Chem., Int. Ed.* **2014**, 53 (52), 14363–14367.
- (42) Greciano, E. E.; Matarranz, B.; Sánchez, L. Pathway Complexity Versus Hierarchical Self-Assembly in N-Annulated Perylenes: Structural Effects in Seeded Supramolecular Polymerization. *Angew. Chem., Int. Ed.* **2018**, *57* (17), 4697–4701.
- (43) Haedler, A. T.; Meskers, S. C. J.; Zha, R. H.; Kivala, M.; Schmidt, H.-W.; Meijer, E. W. Pathway Complexity in the Enantioselective Self-Assembly of Functional Carbonyl-Bridged Triarylamine Trisamides. J. Am. Chem. Soc. 2016, 138 (33), 10539–10545.